Photon-decay modes of the giant dipole resonance in even-A Nd isotopes

S. D. Hoblit* and A. M. Nathan
Nuclear Physics Laboratory and Department of Physics, University of Illinois at Urbana-Champaign, Champaign, Illinois 61820
(Received 15 July 1991)

The photon-decay modes of the giant dipole resonance (GDR) in the nuclei ^{142,146,148,150}Nd were investigated via elastic and inelastic photon scattering. Considerable inelastic scattering was seen into the first excited state of each nucleus. In ^{148}Nd and ^{150}Nd, scattering into several higher levels was also resolved and found to be quite weak. The data are interpreted in the context of both the dynamic collective model and interacting boson model. In these models, the photon decays of the GDR to excited states are a consequence of the coupling between the giant resonance and collective surface degrees of freedom, such as rotations and vibrations. The present data provide the first experimental test of the photon-decay predictions of these models across an entire transitional chain. Both models give an excellent account of the data.

I. INTRODUCTION

This paper reports a photon-scattering study of the photon-decay modes of the giant dipole resonance (GDR) in the transitional chain of Nd isotopes. The motivation for this work is to test nuclear structure models that predict these decay modes based on the coupling between the GDR and low-lying collective levels. It has long been believed that one of the primary mechanisms for the damping of collective giant multipole strength is through the coupling to low-lying collective degrees of freedom, such as quadrupole or octopole surface vibrations. In particular, there is considerable evidence that the GDR is strongly coupled to collective quadrupole surface vibrations and that this coupling often dominates the structure of the GDR, especially in medium and heavy nuclei [1]. The consequences of this coupling are the mixture of surface vibrational components into the GDR state, the fractionation and consequent spreading of the GDR into vibrational satellite peaks, and the acquisition of often substantial branching ratios for photon emission from the GDR to low-lying vibrational levels. Photon scattering is an ideal reaction for probing the coupling of the dipole and quadrupole modes, since photons strongly and selectively excite the dipole mode and since inelastic scattering to vibrational states provides a direct measure of the mixture of vibrational components into the wave function of the GDR.

Historically, the first attempt to describe the coupling quantitatively was the hydrodynamic model and its extension, the dynamic collective model (DCM) [2], where the coupling is a consequence of the hydrodynamic result that the frequency of the dipole mode of a liquid drop is proportional to the inverse of the radius of the drop. This leads to the well-documented scaling of the GDR energy with $A^{-1/3}$ as well as the energy splitting of the resonance in nuclei with a static deformation. For nuclei with a vibrating surface, this leads to an almost classical problem of the coupling between high-frequency dipole modes and low-frequency surface modes, resulting in an admixture of surface vibrational components into the GDR state. Qualitatively, for nuclei that are "soft" vibrators (i.e., low frequency and large amplitude), one expects a strong coupling between the dipole mode and surface vibrations, a large splitting of the dipole strength into satellite peaks, and a substantial photon-decay branch of the GDR to low-lying vibrational levels. The opposite is expected for "stiff" vibrators (i.e., high frequency and small amplitude). The DCM has met with considerable qualitative and quantitative success in predicting the distribution of dipole strength [1] in a wide range of nuclei ranging from spherical vibrators to deformed rotors, including the so-called transitional nuclei which span these two extremes. On the other hand, tests of predictions of photon decays to low-lying vibrational levels, although largely successful, are not very extensive and are limited to a few medium-weight spherical vibrators [3] and heavy deformed rotors [4]. In particular, there has never been a systematic test of the predictions across an entire transitional chain spanning between spherical vibrational nuclei and strongly deformed rotors.

More recently, the interacting boson model (IBM) has been expanded to include the GDR and its coupling to the low-lying collective levels [5,6]. The IBM has enjoyed considerable success over the last decade in predicting the properties of these low-lying levels in a wide range of nuclei throughout the periodic table. Among its more recent accomplishments is the successful prediction of the shape of the photoabsorption cross section in the GDR region of transitional and deformed nuclei [7]. However, there have been few comparisons between theory and experiment with regard to the photon-decay branches. The most detailed comparison to date has been for inelastic photon scattering into the γ band of the strongly deformed nucleus ^{166}Er, where the model was found to be quite successful in accounting for the experimental data [4]. In fact, with a relatively simple version of both the DCM and IBM, it has been shown that both models can account for all the photonuclear data on ^{166}Er. However, as with the DCM, there has never been

 ©1991 The American Physical Society

a systematic test of the predictions of photon-decay branches across a transitional chain.

The even-A Nd isotopes $^{142-150}$Nd are an ideal testing ground for these models. The transitional nature of this chain shows up in various ways, as demonstrated in Figs. 1–3. For example, the energy-level diagrams [8,9] in Fig. 1 indicate that these nuclei exhibit a broad diversity in the structure of their low-lying levels, ranging from the closed $N=82$ neutron shell (^{142}Nd) to classical examples of a nearly harmonic vibrator (^{146}Nd) and of a deformed rotor (^{150}Nd). There is also diversity in the expected strength of coupling between the GDR and surface modes. One can characterize the strength of this coupling by the ratio of the energy of the first excited state E_2 to the parameter β_0 [10], which is proportional to the square root of reduced $E2$ transition rate coupling the ground state to the lowest 2^+ state. For vibrational nuclei β_0 is the zero-point vibrational amplitude, while for deformed nuclei it is the static deformation. In Fig. 2 we show a two-dimensional plot of E_2 vs β_0 for the even-A Nd isotopes. One clearly sees that the expected strength of the coupling to the surface ranges from very weak in the case of ^{142}Nd to very strong in the case of ^{150}Nd. One signature of this coupling should be the broadening of the dipole strength. This is demonstrated in Fig. 3, which shows the measured photoabsorption cross section across the isotopic chain [1]. One sees a gradual broadening of the GDR as the expected strength of the coupling increases across the chain, from the relatively narrow strength distribution in $A=142$ to the more broadened distribution in $A=146$, to the splitting into two modes that is characteristic of deformed nuclei in $A=150$. The

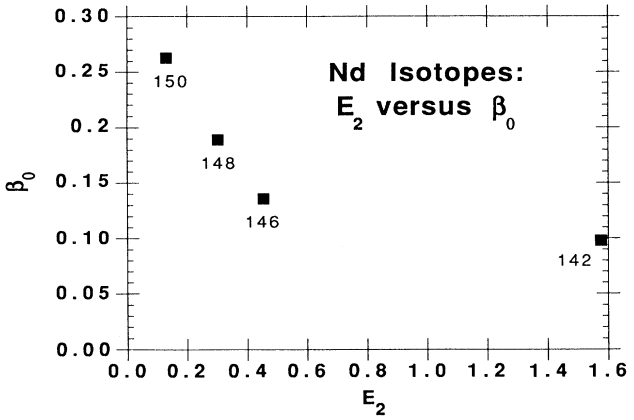

FIG. 2. Two-dimensional plot of the energy of the first excited state vs the parameter β_0 for the Nd isotopes studied. The coupling of the GDR to the nuclear surface modes is expected to be greatest for nuclei in the lower right corner and least for those in the upper left corner.

preceding considerations lead us to expect also a broad diversity across the chain in the photon-decay branches to the first few excited states. It is the purpose of the present work to test both our general ideas about the coupling as well as the specific nuclear structure models by measuring the photon-decay branches, mainly to the first excited state.

The remainder of the paper is organized as follows. In Sec. II we briefly discuss the experimental procedures and data reduction. In Sec. III we describe the DCM and

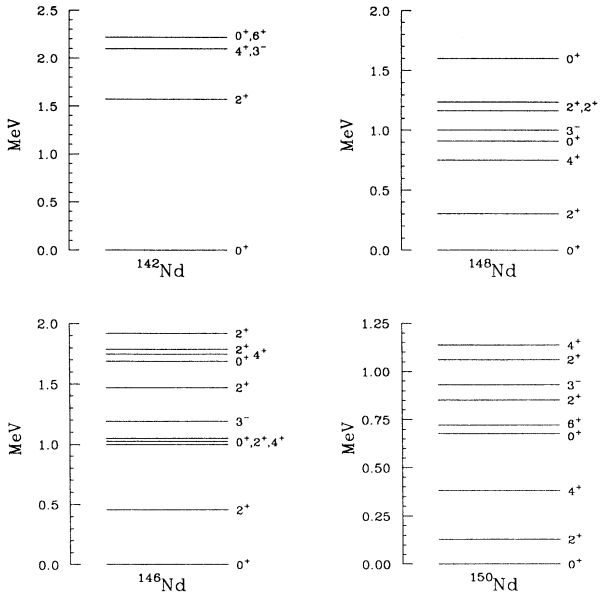

FIG. 1. Selected low-lying states in the even-A Nd isotopes studied.

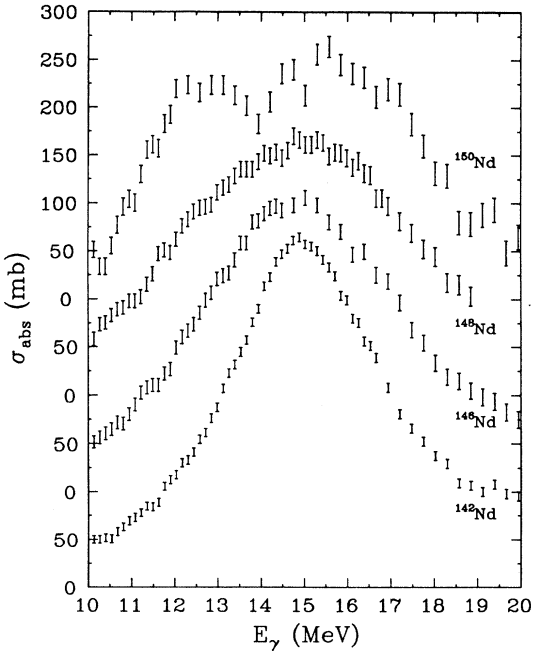

FIG. 3. Experimental values [1] of the photoabsorption cross sections for the Nd isotopes.

IBM as well as the formalism whereby one uses these models to calculate photon-scattering and photoabsorption cross sections. In Sec. IV we analyze and discuss our results in light of the comparison between the measured cross sections and model calculations. In Sec. V we summarize our results and reiterate our principal conclusions.

II. EXPERIMENTAL TECHNIQUE

The main experimental challenge in measuring the photon-scattering cross sections is in achieving a combined energy resolution in the incident photon beam and photon detector sufficient to separate the inelastic scattering from the much stronger elastic scattering. We accomplished this by using incident beams of quasimonochromatic photons produced at the University of Illinois tagged-photon facility and large-volume, good-energy-resolution NaI(Tl) spectrometers to detect the scattered photons. The tagged-photon technique has been previously described [11,12], and we only highlight the discussion here. The experimental setup is shown schematically in Fig. 4. An incident electron beam of energy 24.1 MeV is provided by the 100% duty factor MUSL-2 accelerator. This strikes a 34.3-mg/cm^2 Al foil where a small percentage of the incident beam emits bremsstrahlung photons. The post-bremsstrahlung electrons are momentum analyzed in a double-focusing magnetic spectrometer and detected in an array of plastic scintillators, thereby tagging the associated photons and sorting them into 32 contiguous 100-keV-wide energy bins. A valid event is defined to be a time-correlated coincidence between a tagging electron and a photon which scatters from the scattering target into the NaI spectrometer. The experimental technique involves a two-part measurement, as shown in Fig. 4. First, the NaI is placed directly into the tagged-photon beam in order to calibrate the bremsstrahlung flux and measure the response of the NaI to quasimonochromatic photons. Second, the NaI is placed at an appropriate angle in order to view only those photons that have scattered from the target. The data-acquisition software sorts the NaI pulse height into a total coincidence or an accidental coincidence spectrum, depending on the time difference between the detection of the photon in the NaI and the detection of the associated electron in a focal-plane counter. The net coincidence spectra are generated off line by subtracting an appropriate amount of the accidental coincidences from the total coincidences.

The primary photon detector consisted of a 24-cm-diam by 36-cm-long cylinder of NaI, surrounded by an 11-cm-thick plastic anticoincidence shield. The shield served to improve the energy resolution by rejecting events in which some of the electromagnetic shower escaped from the NaI and into the plastic. The detector observed photons which scattered at an angle of either

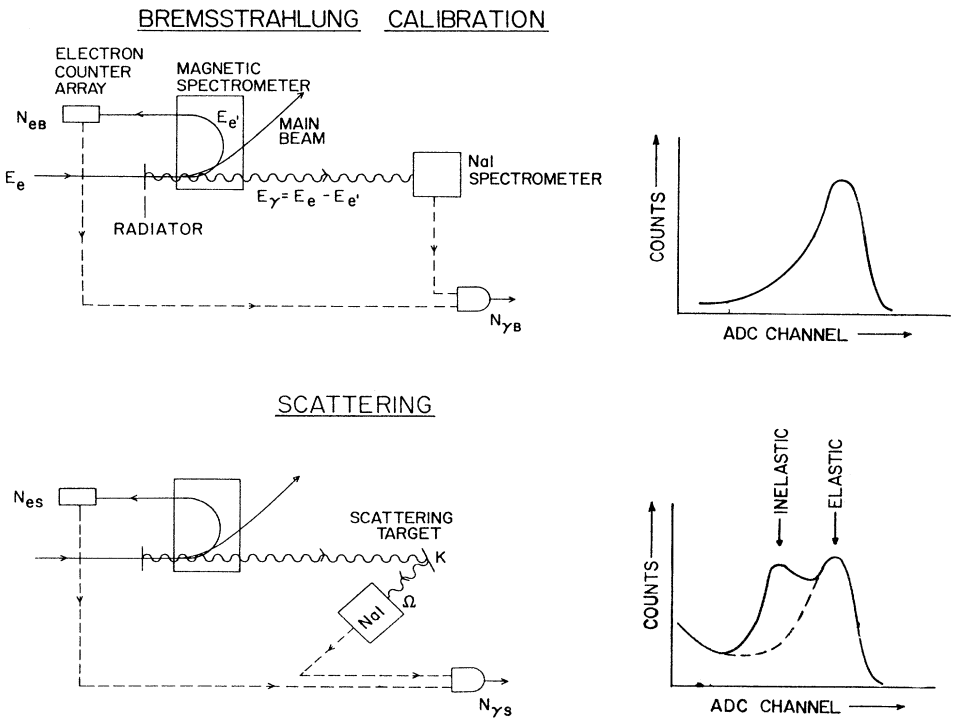

FIG. 4. Schematic representation of the photon-tagging procedure, showing the bremsstrahlung calibration and photon-scattering configurations. $N_{\gamma B}$ and $N_{\gamma S}$ indicate the number of events detected in the two experiments, and N_{eB} and N_{eS} represent the total number of electrons counted in a given tagging channel.

90° or 79° and was able to be rotated to 0° for the bremsstrahlung calibration. A secondary NaI(Tl) detector, 24 cm in diameter by 30 cm long, was used at a fixed backward angle of 144° for the ^{150}Nd measurements. No anticoincidence shield was used for this detector. Both crystals were surrounded by 2.5 cm of $^{6}Li_2CO_3$, which is an effective absorber of low-energy neutrons, and 11.4 cm of lead. Typical energy resolutions achieved in the primary detector were 2.3% full width at half maximum.

The Nd targets were isotopically enriched and in the form of oxide powders (Nd_2O_3). The amount of each isotope used and the percentage enrichments are given in Table I. The powders were packed into thin-walled (2-mm) Lucite boxes shaped to simplify the determination of target absorption effects. These effects as well as the detector efficiency, effective solid angle, and effective target thickness were calculated using a Monte Carlo code [12] based on the electromagnetic shower code EGS4 [13]. Two different magnet settings were used with the tagging spectrometer, spanning photon energies from 12 to 15 and from 15 to 18 MeV. There was an overlap of a few hundred keV near 15 MeV, which provided an internal consistency check on the cross sections. Both tagging intervals included the 15.1-MeV resonance fluorescence line in carbon, which was present because of the Lucite target boxes. This line served as a convenient on-line monitor of both the line shape and gain of the NaI spectrometers.

TABLE I. Percentage enrichments and amounts of the isotopes studied.

Isotope	Weight of Nd_2O_3 (g)	Isotopic enrichment (%)
^{142}Nd	150.7	96.3
^{146}Nd	160.6	95.5
^{148}Nd	81.9	94.1
^{150}Nd	87.8	93.9

Typical pulse-height spectra for each isotope are shown in Fig. 5. In ^{142}Nd the first excited state lies 1.576 MeV above the ground state, thereby allowing for a clean separation between the scattering to this state and the

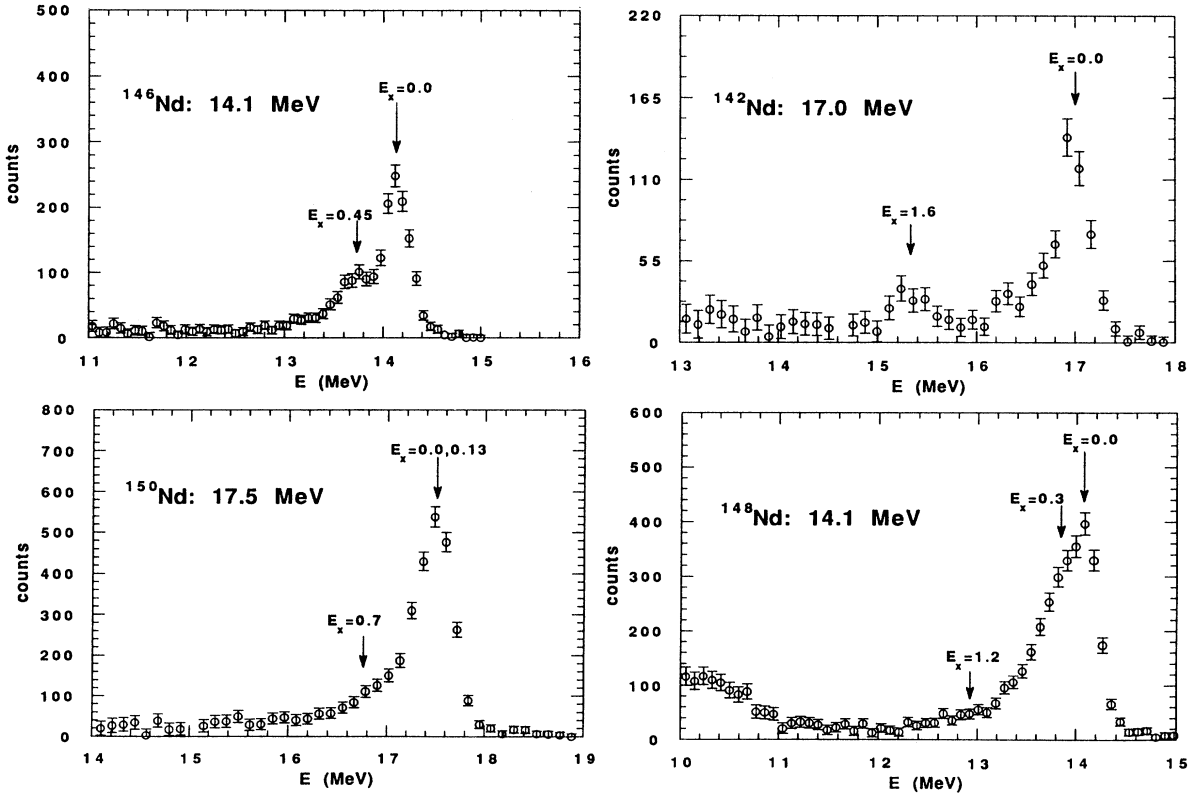

FIG. 5. Typical spectra of scattered photons. The arrows identify expected locations of peaks corresponding to scattering leaving the nucleus with excitation energy E_x. The scattering into the first excited state is clearly resolved in both ^{142}Nd and ^{146}Nd. In ^{148}Nd the scattering into the first excited state is not directly resolved from the elastic scattering; instead, the two peaks appear as a single peak much broader than that expected for elastic scattering alone. In ^{150}Nd the two peaks are indistinguishable from that expected for a single peak. Scattering into levels higher than the first excited state is inferred only by a careful line-shape analysis of the scattering spectra.

elastic scattering. In ^{146}Nd the scattering into the first excited state at 454 keV lies very close to the small but non-negligible one-escape peak from the elastic scattering. In ^{148}Nd the first excited state is only 302 keV above the ground state, and elastic and inelastic scattering appear as a single broadened peak. In all three cases, the inelastic scattering was separated using a maximum-likelihood, multipeak fit to the spectra, using line shapes calculated with our Monte Carlo code. These line shapes were calibrated against the line shapes measured with the detector placed directly into the photon beam and checked against the 15.1-MeV resonance fluorescence line. For ^{142}Nd and ^{146}Nd, no evidence was found for inelastic scattering into levels other than the first excited state, whereas in ^{148}Nd a weak transition to the 2_2^+ state was found.

For ^{150}Nd, the first excited state is only 130 keV above the ground state and scattering into this state cannot be resolved from elastic scattering. Instead, we relied on the fact that the elastic scattering has a different angular distribution $(1+\cos^2\theta)$ than the scattering into a 2^+ level $(13+\cos^2\theta)$ in order to separate the two contributions. Therefore, scattering data were taken at both 79° and 144° using the two-detector setup, and the data were analyzed as a single "quasielastic" peak. Scattering into the γ bandhead at 1.06 MeV and unresolved scattering into the 0.68- and 0.85-MeV members of the β band were energetically resolved from the scattering into the ground-state band and found to be very weak, as shown in Fig. 5 for the case of scattering into the β band.

III. FORMALISM FOR THE ANALYSIS

A. Overview

We interpret our data in the context of both the DCM and IBM. In each case a model Hamiltonian is diagonalized, yielding the energies and wave functions of both the low-lying collective states (rotations and vibrations) and the higher-lying GDR states, as well as the dipole matrix elements coupling the two sets of states. These energies and matrix elements are then used to calculate elastic and inelastic photon-scattering cross sections. In this section we present an overview of the physics of each model, as well as the formalism relating the nuclear structure information to the scattering and photoabsorption cross sections.

B. Dynamic collective model

The algebraic structure of the DCM Hamiltonian is based on the geometry of the hydrodynamic model. This model describes the GDR as the oscillation of a liquid drop with a constant density in the interior. The additional requirement of a well-defined nuclear surface leads to a boundary condition that requires the energy of the dipole mode to be inversely proportional to the nuclear radius, thereby giving rise to a natural coupling between the dipole mode and surface degrees of freedom. A signature for this coupling is the photon decay of the giant dipole resonance into the low-lying vibrational states.

The full DCM Hamiltonian is given by

$$\mathcal{H}_{\rm DCM}=H_{\rm rot\text{-}vib}+H_{\rm dip}+H_{\rm int}\ . \tag{1}$$

In the usual tensorial notation, the Hamiltonian describing the low-lying rotational and vibrational degrees of freedom, $H_{\rm rot\text{-}vib}$, is given by [14]

$$\begin{aligned}H_{\rm rot\text{-}vib}=&P_2[\pi^{[2]}\times\pi^{[2]}]^{[0]}\\&+P_3[[\pi^{[2]}\times\alpha^{[2]}]^{[2]}\times\alpha^{[2]}]^{[0]}+\cdots\\&+C_2\hat{L}_2+C_3\hat{L}_3+C_4\hat{L}_2^2+C_5\hat{L}_2\hat{L}_3+C_6\hat{L}_3^2\\&+D_6\hat{L}_2^3+\cdots\ ,\end{aligned} \tag{2}$$

with

$$\begin{aligned}\hat{L}_2&=[\alpha^{[2]}\times\alpha^{[2]}]^{[0]}\ ,\\ \hat{L}_3&=[\alpha^{[2]}\times\alpha^{[2]}\times\alpha^{[2]}]^{[0]}\ ,\end{aligned} \tag{3}$$

where the $\alpha^{[2]}$ are the quadrupole vibrational amplitudes and the $\pi^{[2]}$ are the conjugate momenta. The coupling of the various tensors to total angular momentum zero ensures the rotational invariance of the Hamiltonian. This Hamiltonian potentially allows for the description of a great variety of collective nuclear motion, ranging from anharmonic vibrators to deformed rotors to gamma-unstable nuclei to triaxial nuclei. Typically, one adjusts the P_i and C_i in order to fit the energies and electromagnetic decay properties of the low-lying levels. However, for reasons to be discussed below, we limit $H_{\rm rot\text{-}vib}$ to purely harmonic vibrational and rotational terms. Therefore, only the terms involving P_2 and C_2 are present, and these terms alone are sufficient to determine the vibrational spectrum and decay properties. The GDR Hamiltonian $H_{\rm dip}$ is also treated in the harmonic approximation and is therefore given by

$$H_{\rm dip}=B_1^{-1}[\pi^{[1]}\times\pi^{[1]}]^{[0]}+C_1[q^{[1]}\times q^{[1]}]^{[0]}\ . \tag{4}$$

Together, B_1 and C_1 determine both the unperturbed energy of the GDR and the integrated dipole strength and are usually adjusted to fit those quantities. The interaction Hamiltonian [14] coupling the quadrupole and dipole degrees of freedom, $H_{\rm int}$, can be expanded in a power series in the surface vibrational amplitudes $\alpha^{[2]}$. The leading terms in this expansion are

$$\begin{aligned}H_{\rm int}=&V_1[[q^{[1]}\times q^{[1]}]^{[2]}\times\alpha^{[2]}]^{[0]}\\&+V_{00}[\alpha^{[2]}\times\alpha^{[2]}]^{[0]}[q^{[1]}\times q^{[1]}]^{[0]}\\&+V_{22}[[\alpha^{[2]}\times\alpha^{[2]}]^{[2]}\times[q^{[1]}\times q^{[1]}]^{[2]}]^{[0]}\ .\end{aligned} \tag{5}$$

Although the algebraic structure of this interaction is quite general, the V parameters are model dependent. In the liquid-drop model, these parameters are *uniquely* specified [2] in terms of C_1 and B_1. Therefore, once the dipole and quadrupole Hamiltonians are specified in the manner discussed above, the DCM interaction Hamiltonian is completely determined.

As mentioned above, all our interpretations are based on the assumption of harmonicity for the surface vibrations. This limits us to two extreme cases: spherical har-

monic vibrators and well-deformed axially symmetric rotors. The reason for this limitation is purely technical. The DCM was originally developed for these two extreme cases alone. Only later was it extended to the case of more general collective motion. Unfortunately, the rather complicated computer codes needed for the general case are no longer available. Nevertheless, despite the obvious transitional nature of the Nd chain, we will show that the calculations done under the extreme assumptions give a remarkably good account of the data. Further, the more general cases can now be done with considerably more calculational ease using the IBM.

C. Interacting boson model

In the IBM, the low-lying collective states are described as interacting bosons of spins 0 and 2 or s and d bosons. The GDR is described as a spin-1 p boson. The Hamiltonian of the low-lying states and their interaction with the dipole states is constructed using general group-theoretical techniques. In the usual second-quantized formalism, the full Hamiltonian assumes the general form

$$\mathcal{H}_{\rm IBM}=H_{sd}+H_p+H_{\rm int} \ . \tag{6}$$

The form of the sd Hamiltonian is given by [7]

$$H_{sd}=\epsilon\hat{n}_d+a_0(\hat{P}^\dagger\cdot\hat{P})+a_1(\hat{L}\cdot\hat{L})+a_2(\hat{Q}\cdot\hat{Q}) +a_3(\hat{T}_3\cdot\hat{T}_3)+a_4(\hat{T}_4\cdot\hat{T}_4) \ , \tag{7}$$

where

$$\hat{n}_d=(d^\dagger\cdot\tilde{d}) \ ,$$
$$\hat{P}=\tfrac{1}{2}(\tilde{d}\cdot\tilde{d})-\tfrac{1}{2}(\tilde{s}\cdot\tilde{s}) \ ,$$
$$\hat{L}=\sqrt{10}(d^\dagger\times\tilde{d})^{(1)} \ ,$$
$$\hat{Q}=(s^\dagger\times\tilde{d}+d^\dagger\times\tilde{s})+\chi(d^\dagger\times\tilde{d})^{(2)} \ ,$$
$$\hat{T}_3=(d^\dagger\times\tilde{d})^{(3)} \ ,$$
$$\hat{T}_4=(d^\dagger\times\tilde{d})^{(4)} \ ,$$

with $\tilde{d}_\mu\equiv(-1)^\mu d_{-\mu}$ and $\tilde{s}\equiv s$. The IBM does not determine the coefficients ϵ and a_i in Eq. (7). These are usually adjusted to fit the properties of the low-lying levels. As in the full DCM Hamiltonian, H_{sd} can describe a great variety of collective behavior, but unlike the DCM, the calculations can be done with relative ease. Thus, in the calculations to be described below, the full complexity of H_{sd} will be used, which should be of particular value in studying the transitional Nd chain. The inclusion of a p boson with $J=1$ [6] leads to H_p with the particularly simple form

$$H_p=\epsilon_p(p^\dagger\cdot\tilde{p}) \ , \tag{8}$$

with the parameter ϵ_p adjusted to fit the energy of the GDR. The interaction Hamiltonian $H_{\rm int}$ between the GDR and low-lying states is given by

$$H_{\rm int}=b_0(d^\dagger\times\tilde{d})^{(0)}\cdot(p^\dagger\times\tilde{p})^{(0)}+b_1(d^\dagger\times\tilde{d})^{(1)}\cdot(p^\dagger\times\tilde{p})^{(1)} +b_2[(s^\dagger\times\tilde{d}+d^\dagger\times\tilde{s})^{(2)} +\chi_p(d^\dagger\times\tilde{d})^{(2)}]\cdot(p^\dagger\times\tilde{p})^{(2)} \ . \tag{9}$$

Unlike the DCM, there is as yet no theoretical guidance as to the specification of the coupling parameters (the b's and χ_p), and so one must resort to adjusting these parameters to fit some body of data. However, one expects that the parameters vary only very slowly from nucleus to nucleus within an isotopic chain. Therefore, there is reason to hope that the theory has real predictive power. We have not attempted to determine these parameters ourselves; rather, we use schemes presented in the literature, as discussed below. At this point we remark that the most important term in $H_{\rm int}$ is the one involving b_2. In deformed nuclei, for example, it is this term that determines the splitting between the two dipole modes [4] and is analogous to the term involving V_1 in the DCM [Eq. (5)]. A careful comparison between Eqs. (7) and (9) reveals that the coupling implied by the b_2 term is through the sd-quadrupole operator $\hat{Q}$, provided that $\chi_p=\chi$. Motivated by the geometrical picture of the DCM in which the principal coupling is through quadrupole deformations, we assume that this relation is obeyed. This is an extension of the so-called "consistent Q formalism." As originally applied, the same form for the quadrupole operator was used both in H_{sd} and in the $E2$ operator [15]. Here we extend the same form to $H_{\rm int}$ [4,16].

D. Relation to photon-scattering cross sections

The diagonalization of the interaction Hamiltonians in the various models yields dipole energies E_n and the wave functions of both the low-lying states, $|I_f^+\rangle$, and dipole states, $|1_n^-\rangle$. These are then used to calculate dipole transition strengths connecting the dipole to the low-lying states, $\langle 1_n^-||\mathbf{D}||I_f^+\rangle$, which are related to the cross sections as follows [14]:
(i) absorption,

$$\sigma_{\rm abs}=\frac{4\pi E}{\sqrt{3}\hbar c}{\rm Im}P_0 \ ; \tag{10}$$

(ii) scattering,

$$\frac{d\sigma_{0^+\to I_f^+}(E,\theta)}{d\Omega}=\frac{E'}{E}|P_j|^2 g_j(\theta)\delta_{jI_f} \ , \tag{11}$$

where the angular distributions are given by

$$g_0(\theta)=\tfrac{1}{6}(1+\cos^2\theta) \ ,$$
$$g_2(\theta)=\tfrac{1}{12}(13+\cos^2\theta) \ .$$

Here θ is the scattering angle and E and E' are the energies of the incident and scattered photons, respectively. The polarizabilities are given by

$$P_j=\delta_{jI_f}\frac{1}{\sqrt{3(2I_f+1)}}\frac{EE'}{(\hbar c)^2}\sum_n\langle I_f^+||\mathbf{D}||1_n^-\rangle\langle 1_n^-||\mathbf{D}||0^+\rangle\left[\frac{1}{E_n+E'+\frac{1}{2}i\Gamma_n}+\frac{1}{E_n-E-\frac{1}{2}i\Gamma_n}\right]-\delta_{j0}\delta_{f0}\sqrt{3}\frac{(Ze)^2}{AMc^2}\ . \tag{12}$$

Neither model specifies the damping widths Γ_n of the GDR states. These widths arise from the coupling of the collective GDR states to more complicated degrees of freedom. We parametrize these widths according to the phenomenological prescription of Danos and Greiner [17],

$$\Gamma_n=\Gamma_0(E_n/E_0)^\delta\ , \tag{13}$$

where Γ_0 and δ are justified to fit the scattering data. It is worth stressing that these poorly known damping widths have a major effect on the cross sections, including the amount of inelastic scattering. As we will see, they represent an important limitation in our ability to use the scattering cross sections to discriminate among different structure models. We iteratively adjusted the width parameters to fit the elastic-scattering data of the entire chain of isotopes for each model. We arrived at the parameters

$$\Gamma_0=2.6\ \text{MeV},\quad \delta=1.3,\quad E_0=12\ \text{MeV}\ ,$$

which we then used for all isotopes and for both models in comparing the theory to the data. Fixing the parameters once and for all hopefully allows a more meaningful comparison between the models and data. We allowed two additional parameters to vary during the fitting procedure: the unperturbed energy of the GDR and the overall normalization scale of the cross sections. The normalization adjustment simply reflects the fact that our main interest in the data is the relative amounts of elastic and inelastic scattering as a function of energy, which this overall normalization parameter preserves, and not the absolute scale of the cross sections. Finally, as we shall show, our measured scattering cross sections are not consistent either in shape or in magnitude with the total photoabsorption cross sections [1]. We do not attempt to resolve these discrepancies, but rather take our data as a consistent set and base our calculations and conclusions on them exclusively.

IV. ANALYSIS AND DISCUSSION

Calculations were performed along the lines indicated in the preceding section. For the DCM the calculations assumed that ^{142}Nd and ^{146}Nd can be described as spherical vibrators and that ^{150}Nd can be described as a de-

TABLE II. Parameters specifying the spherical DCM in the various nuclei.

Isotope	$E_{2_1^+}$ (MeV)	β_0	E_{GDR} (MeV)
^{142}Nd	1.576	0.098	14.78
^{146}Nd	0.454	0.136	14.73
^{148}Nd	0.302	0.189	14.23

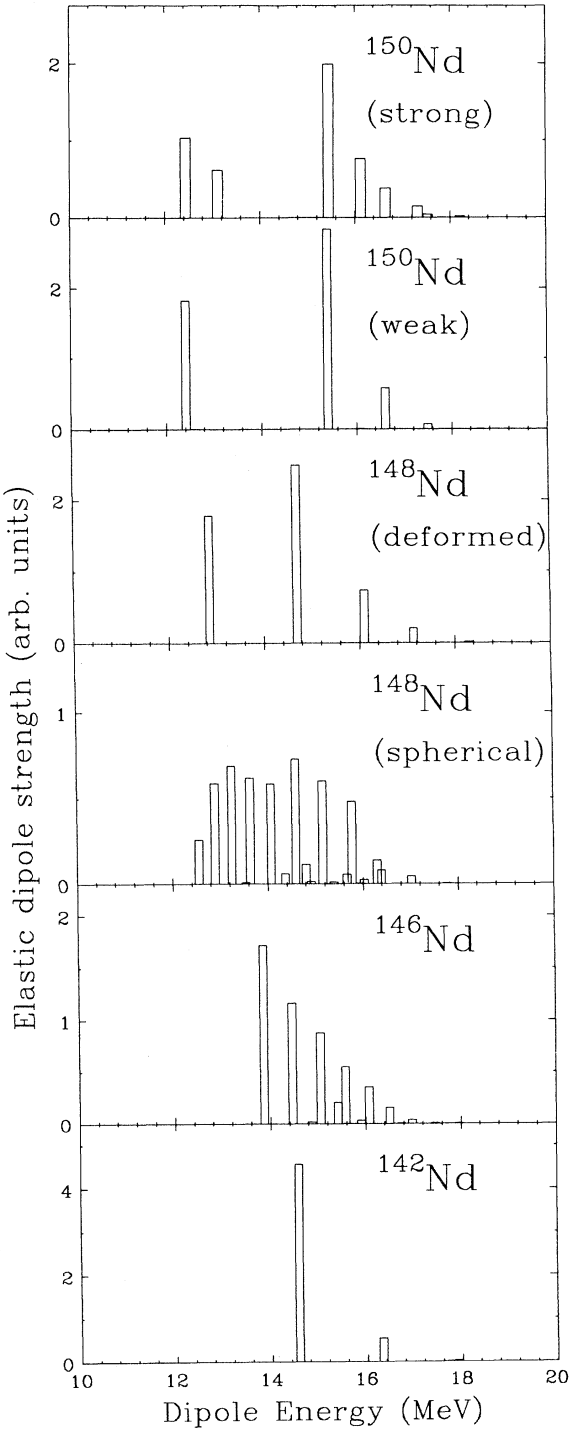

FIG. 6. Distribution of dipole strength between the ground and dipole states calculated using the DCM. For ^{148}Nd the distribution is calculated under both the deformed and spherical hypotheses. For ^{150}Nd the distribution is calculated for both weak and strong coupling to β vibrations, as discussed in the text.

TABLE III. Parameters specifying the deformed DCM for the various nuclei modeled. All energies are in units of MeV.

Isotope	$E_{2_1^+}$	E_γ	E_β	β_0	$\bar{\gamma}$	$\overline{\beta-\beta_0}$	E_{GDR}
^{148}Nd	0.302	1.24	0.91	0.189	17.7°	0	14.47
^{150}Nd	0.130	1.06	0.68	0.263	12.4°	0.019–0.058	14.68

formed rotor. For the transitional nucleus ^{148}Nd, we do both the spherical and deformed calculations. For the vibrational cases, only two parameters are needed to specify the surface vibrations, and we take these to be the experimental values [8] of E_2 and the zero-point amplitude β_0. These are listed in Table II along with E_{GDR}, the unperturbed energy of the GDR, which was determined from a fit to the elastic-scattering data. Additional details of similar calculations for vibrational nuclei are given elsewhere [3]. For the deformed cases, E_2 and β_0 are needed to specify the rotational frequency and static deformation, which are sufficient for calculating the coupling to the ground-state rotational band. We also want to calculate the coupling to β and γ vibrations. Assuming the harmonic approximation for those vibrations, we need the energies E_γ and E_β, which are taken directly from known levels, and the zero-point vibrational amplitudes $\overline{\beta-\beta_0}$ and $\bar{\gamma}$. These latter quantities are derived from the reduced $E2$ transition rates coupling the excited

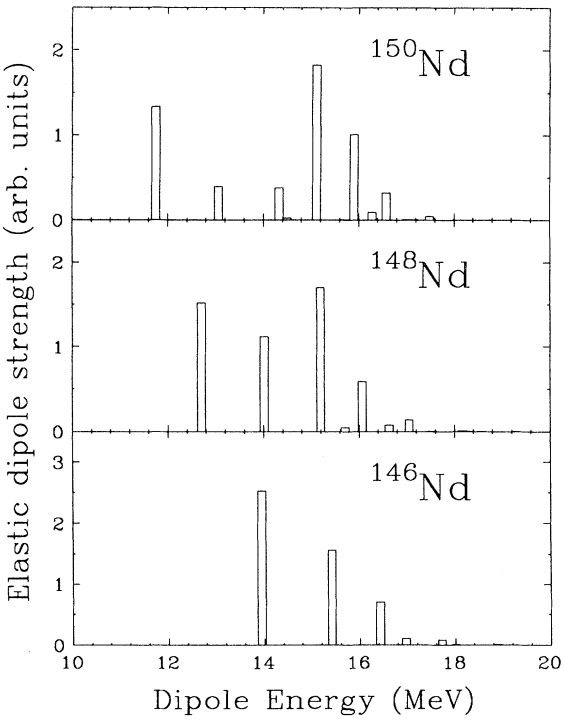

FIG. 7. Distribution of dipole strength between the ground and dipole states calculated using the IBM.

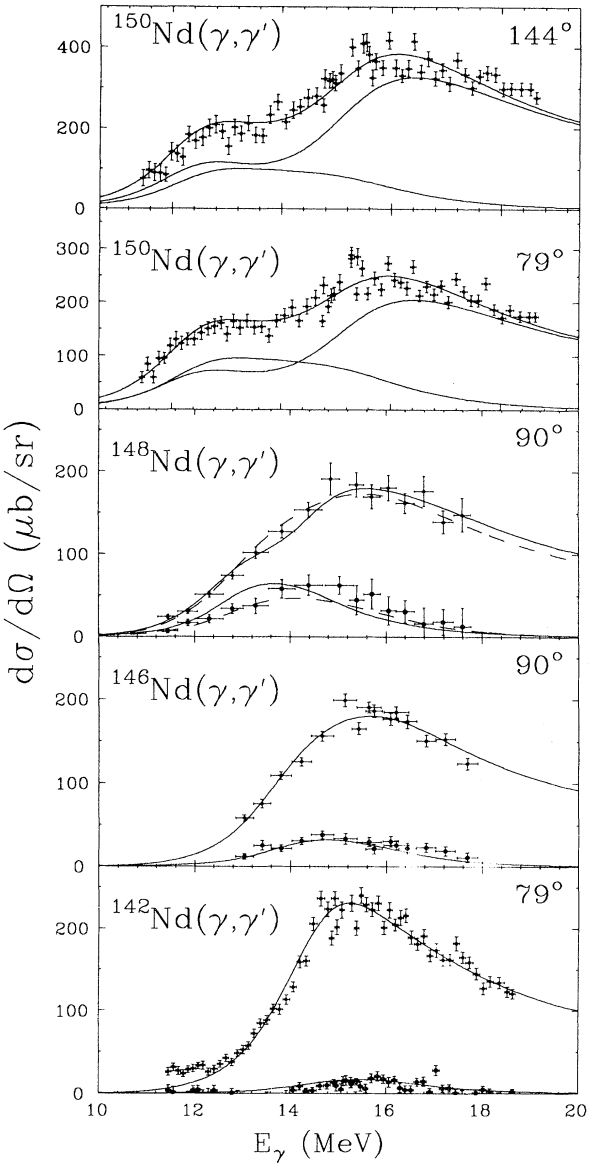

FIG. 8. Photon-scattering cross sections into the ground and first excited states with the results of the DCM calculations. For ^{148}Nd the solid and dashed curves are calculations under the deformed and spherical hypotheses, respectively. For ^{150}Nd the inelastic scattering into the first rotational 2^+ state is not resolved from the elastic scattering. Shown are the predicted elastic and inelastic cross sections and their sum.

TABLE IV. Parameters used in specifying the *sd* part of the IBM Hamiltonian in the nuclei studied.

Isotope	N_{bosons}	ϵ	a_0	a_1	a_2	a_3	a_4	χ
^{146}Nd	7	0.6238	−0.0390	0.0055	−0.0162	0.0459	0.0793	−0.6
^{148}Nd	8	0.5486	−0.0131	0.0016	−0.0203	0.0221	0.0530	−1.0
^{150}Nd	9	0.3478	0.0131	0.0006	−0.0161	−0.0144	0.0398	−1.1

band to the ground-state band [4]. For ^{150}Nd these transitions are experimentally known, whereas for ^{148}Nd we have to rely on a theoretical model [2] since the appropriate $E2$ transition rates are not well known. The parameters for the deformed nuclei [8] are given in Table III. Additional details of similar calculations for deformed nuclei are given elsewhere [4]. For the IBM calculations, we have taken input parameters from the literature that had already been optimized to fit energies and electromagnetic decay properties of the low-lying states and total photoabsorption cross section. Of the four sets of parameters we investigated, the best at describing both the low-lying energy levels and our cross sections were those of Maino *et al.* [16]. Their parameters, listed in Tables IV and V, utilize the consistent Q formalism (i.e., $\chi_p=\chi$). No IBM calculations were attempted for ^{142}Nd,

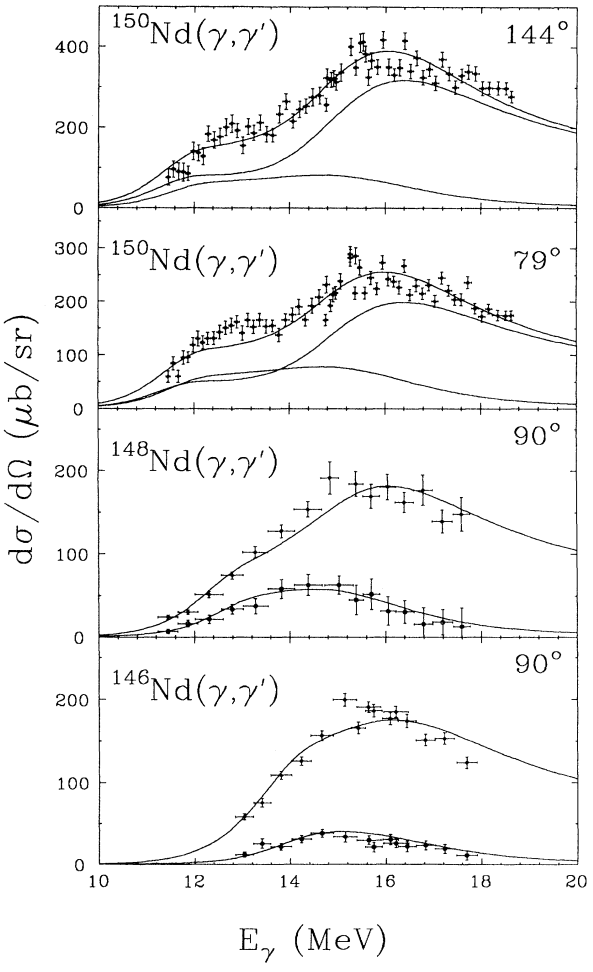

FIG. 9. Photon-scattering cross sections into the ground and first excited states with the results of the IBM calculations. In ^{150}Nd the inelastic scattering into the first rotational 2^+ state is not resolved. Shown are the predicted elastic and inelastic cross sections and their sum.

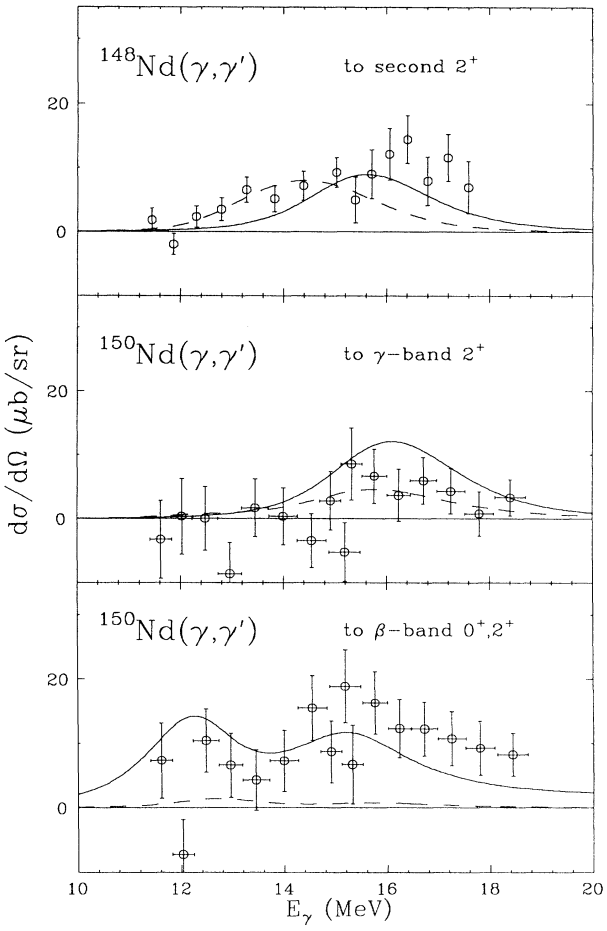

FIG. 10. Photon scattering into higher levels of ^{148,150}Nd. For the scattering cross sections into the 2^+_γ level of ^{150}Nd, the curves are the predictions of the DCM (solid) and IBM (dashed). For the scattering cross sections into the β band of ^{150}Nd, the solid and dashed curves are the predictions of the DCM assuming strong and weak coupling, respectively, between the ground-state and β bands. For the scattering cross sections into the 2^+_2 level of ^{148}Nd, the solid and dashed curves are the predictions using the deformed and spherical versions of the DCM, respectively.

TABLE V. Parameters used in specifying the GDR part of the IBM Hamiltonian in the nuclei studied. The parameter $b_1=0$ for all nuclei.

Isotope	ϵ_p	b_0	b_2	χ_p
^{146}Nd	14.82	0.40	0.65	−0.6
^{148}Nd	14.24	0.40	0.65	−1.0
^{150}Nd	14.00	0.40	0.65	−1.1

which has a closed neutron shell ($N=82$) and therefore lies outside the realm of validity of the model.

The results of the calculations are summarized in Figs. 6–11. In Figs. 6 and 7 we show the calculated distribution of ground-state dipole strength for the DCM and IBM, respectively. In Figs. 8 and 9 we show the measured cross sections for scattering into the ground and first excited states, together with the DCM and IBM calculations, respectively. In Fig. 10 we show the cross sections for inelastic scattering into higher excited states of ^{148}Nd and ^{150}Nd. Finally, in Fig. 11 we compare the photoabsorption cross sections inferred from the elastic-scattering data to photoabsorption data from the literature [1]. We now discuss each nucleus separately.

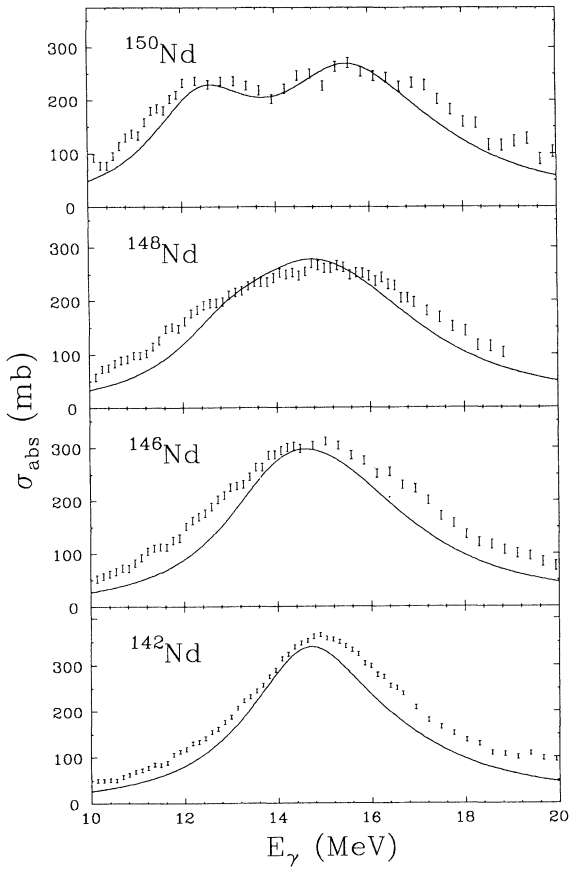

FIG. 11. Comparison between photoabsorption data [1] and photoabsorption cross sections calculated using the DCM.

A. ^{142}Nd

This very stiff vibrational nucleus is expected to be the classic case of weak coupling between the GDR and surface vibrations, since E_2 is high (1.6 MeV) and β_0 is small (≈ 0.1). This expectation is realized by the DCM calculation, which indicates that most of the dipole strength is concentrated in a single peak, with only one very weak vibrational satellite (Fig. 6). Both the calculation and elastic-scattering data confirm this relatively narrow distribution of dipole strength. The weak coupling is also reflected in the inelastic scattering to the 2_1^+ state, which is predicted and measured to be small. The overall agreement between the scattering data and the calculation is excellent.

B. ^{146}Nd

This nucleus is a beautiful example of a soft harmonic spherical vibrator. It offers an interesting contrast to ^{142}Nd since the lower E_2 (0.45 MeV) and larger β_0 (0.14) lead one to expect a considerably greater coupling between dipole and surface modes. Consequently, one expects both a greater fractionation of the dipole strength and a significantly greater amount of inelastic scattering. Both the DCM and IBM confirm our expectations, and both models predict results for the elastic and inelastic cross sections that are remarkably close to the data. Despite this fact, the two models agree only in a qualitative way with each other, as can be seen by a comparison of the distribution of dipole strengths in Figs. 6 and 7. Both calculations indicate a fractionation of the dipole strength into several satellite peaks, extending over an energy of about 2 MeV. However, whereas the IBM has the dipole strength concentrated in three peaks, the DCM has it spread over five or six more closely spaced peaks. These differences between the models are not reflected in the cross sections because they are washed out by the rather large damping widths. This should not be surprising, since the widths are typically 3.5 MeV, which is considerably greater than the separation between the satellite peaks. The cases of ^{142}Nd and ^{146}Nd are qualitatively very similar to the cases of ^{92}Mo and ^{96}Mo, respectively, which were the object of an earlier scattering study [3].

C. ^{150}Nd

This nucleus is very typical of the rare-earth deformed rotors. The low-lying rotational-vibrational properties and GDR are very similar to those of ^{166}Er, which has been the object of considerable study in the literature [4,18]. In deformed nuclei the distribution of dipole strength and the scattering into the ground-state rotational band (both elastic and inelastic) are largely determined by the static deformation. The DCM and IBM agree qualitatively on the distribution of dipole strength: They both predict a splitting into two principal modes (the so-called deformation splitting), with a further splitting into vibrational satellite peaks. However, the two models differ in some details, mainly in the degree of fractionation of the principal modes into satellite states.

These differences are not particularly evident in the scattering into the ground-state band, where both models seem to account for the data at both of the scattering angles. However, the differences are striking in the predictions for the scattering into the 2^+ γ bandhead at 1.06 MeV and into the unresolved 0^+ and 2^+ members of the β band at 0.68 and 0.85 MeV, respectively (see Fig. 10). The scattering into these levels is very weak (typically only a few percent of the scattering into the ground-state band), and the statistical precision is poor, especially for the γ band. Nevertheless, both models seem to account adequately for the scattering data into the γ band, despite the fact that the DCM prediction is a factor of 2 greater than the IBM prediction. It is curious that precisely the same situation occurs for ^{166}Er [4]. It was suggested in that case [4,18] that the difference between the two models is not just due to a different choice of parameters, but is inherent in the structure of the two models. This also seems to be the case with ^{150}Nd. For the DCM the scattering into the γ and β bands in deformed nuclei is a stringent test of the model. To lowest order there is essentially one parameter, V_1 in Eq. (5), which determines the strength of the coupling between the dipole mode and nuclear surface (the other terms are higher order in the vibrational amplitude and therefore less important). Even allowing for a deviation of this parameter from its liquid-drop value, it is largely fixed by the deformation splitting, leaving no additional freedom to account for the coupling to the vibrational bands. This was previously pointed out in the context of the coupling to the γ band in ^{166}Er [4] and applies equally well in the present context. In neither case is the statistical quality of the scattering data into the γ band precise enough to test adequately the DCM or to discriminate between it and the IBM.

The situation is different for the scattering into the β band. In a deformed nucleus, the coupling of the GDR to β vibrations results in a mixing of the GDR's built on the ground-state and β bands, the result of which being that each of the two principal dipole modes develops a vibrational satellite peak. As in the γ-band case, the damping widths wash out the observable effects in the scattering cross sections into the ground-state band; instead, the signature for this coupling is in the inelastic scattering populating the β band. The relevant property of ^{150}Nd that governs the strength with which the GDR couples to the β band is $\overline{\beta-\beta_0}$, the zero-point amplitude for β vibrations. This in turn is experimentally determined by $B(E2;0_g^+\rightarrow 2_\beta^+)$ or $B(E2;0_\beta^+\rightarrow 2_g^+)$. In the pure liquid-drop model, these reduced transition rates should be equal. However, in ^{150}Nd the $0_\beta^+\rightarrow 2_g^+$ transition rate is 10 times the $0_g^+\rightarrow 2_\beta^+$ rate [19,20], despite the fact that the intraband $2\rightarrow 0$ rate is the same for the β band as for the ground-state band. These transitions rates lead to a zero-point amplitude of 0.019 (for the weaker transition) and 0.058 (for the stronger transition). For each of these possible zero-point amplitudes, we have used the DCM to calculate the dipole strength distribution (Fig. 6) and the scattering into the unresolved 0^+ and 2^+ members of the β band (Fig. 10). The results show a vast difference in the predicted scattering cross section for the two cases. The data, although statistically quite poor in quality, show a clear preference for the stronger coupling and suggest that the $0_g^+\rightarrow 2_\beta^+$ transition rate is anomalously small. Other evidence for anomalous behavior of the β band in ^{150}Nd has been previously noted [19]. We remark in passing that the present data represent the first test of the predictions of the DCM for the coupling of the GDR to β vibrations.

D. ^{148}Nd

^{148}Nd lies at the transition between spherical and deformed nuclei. The energy of the first excited state ($E_{2_1^+}=0.302$ MeV) is larger than is typical for deformed rotors in this mass region, but smaller than is typical for spherical vibrators. Likewise, the parameter $\beta_0=0.189$ is small when interpreted as a static deformation, but large when interpreted as a vibrational amplitude. Clearly, this is one case where one would like to do a more general DCM calculation. However, we are forced to compare the scattering data with the extreme versions of the DCM, namely, the deformed and spherical versions, which we now discuss. The distribution of dipole strength is very different for the two calculations (Fig. 6). If the 2_1^+ state is interpreted as a vibration, the large vibrational amplitude leads to a highly fractionated distribution of dipole strength with many closely spaced peaks. On the other hand, if it is interpreted as a rotational level, the distribution is a simple two-peak structure typical of the deformation splitting in deformed nuclei, with a modest fractionation of the upper peak due to the coupling to γ vibrations. Interestingly, despite these two very different distributions of strength, the elastic-scattering data cannot easily distinguish between the extreme possibilities (Fig. 8). The reason is clear: The structure is nearly completely washed out by the damping widths. The differences are somewhat more distinct for the scattering into the 2_1^+ state. The deformed calculation leads to an energy dependence for this cross section that is more compact and peaked at a lower energy than the data. The spherical calculation is in better agreement with the overall shape, although it slightly underestimates the peak of the cross section. Neither calculation completely succeeds in quantitatively accounting for the inelastic cross section.

The scattering into the 2_2^+ level of ^{148}Nd is shown in Fig. 10 along with the two extreme DCM calculations. In the spherical case, the 2_2^+ level is interpreted to be a two-phonon vibration, whereas in the deformed case it is interpreted to be the γ-vibrational bandhead. In the latter case, it is necessary to provide as input the zero-point amplitude. Since the relevant $E2$ transition rates are not known, we instead used a value for the zero-point amplitude equal to 60% of that predicted by the liquid-drop model, as is typical for γ vibrations in this mass region [4]. As in the case of ^{150}Nd, the statistical precision of the data are not good; nevertheless, they show a preference for the deformed interpretation.

On the other hand, the IBM seems to account for the transitional nature of this nucleus in that the distribution

of dipole strength (Fig. 7) is intermediate between that of the deformed ^{150}Nd and spherical ^{146}Nd. This model currently predicts the magnitude and energy dependence of the inelastic scattering into the 2_1^+ state. We view this as a remarkable success of the IBM.

E. Photoabsorption cross sections

In Fig. 11 we compare the photoabsorption cross sections inferred from the scattering data to cross sections measured directly [1]. The curves were calculated using the DCM with input parameters that fit the elastic-scattering data, as discussed above. This figure clearly shows that the present elastic-scattering data are not compatible with the previously measured photoabsorption cross sections. In particular, the scattering data imply a consistently narrower width for the GDR than that implied by the photoabsorption data. We have no explanation for this discrepancy.

F. Discussion

The preceding analysis demonstrates that the surface degrees of freedom play an important role in determining the properties of the GDR, particularly the photon-decay branches. Furthermore, both the DCM and IBM do a remarkably good job describing both qualitative and quantitative features of these decay branches for the transitional chain of Nd isotopes. We now ask whether the photon-scattering data are able to discriminate between these two models. That is, does one model consistently work better than the other in describing the scattering data? If one considers only the scattering into the ground and first excited states, the answer appears to be *no*; i.e., the present analysis shows that the data *cannot* discriminate between the DCM and IBM. Moreover, this inability to discriminate does not seem to be an experimental limitation; better, more precise data will not help the situation. Instead, it seems to be a fundamental limitation, largely a result of the damping widths. A classic example is ^{146}Nd: The two models predict very different distributions of dipole strength, yet very similar scattering cross sections. An even more striking example is ^{148}Nd, where three very different models (the spherical DCM, deformed DCM, and IBM) lead to essentially the *same* predictions for the scattering cross sections into the ground and first excited states. On the other hand, if one considers scattering into higher levels, then precise scattering data could, in principle, distinguish between the predictions of the two models. This was previously noted in the case of scattering into the 2_γ^+ level of ^{166}Er and applies equally well for the scattering into the 2_γ^+ level of ^{150}Nd, where our analysis shows that precisely measured cross sections *could* discriminate between the two models. Unfortunately, the present data for the scattering into the 2_γ^+ level in ^{150}Nd are not precise enough, and no conclusions can be drawn as to the relative merits of the two models. Nevertheless, we believe that such data are potentially very interesting and suggest this as a possible goal for future investigations.

The issue of the coupling of the GDR to the nuclear surface degrees of freedom is closely related to another issue of current interest in nuclear structure physics, namely, the shape of the nuclear surface at high temperature and/or high angular momentum. Through a study of the photon spectrum following the fusion of two heavy ions, it is claimed that the shape of the GDR built on highly excited states can be determined. Because of the close relationship between the shape of the GDR and the shape of the nuclear surface, it is further claimed that the shape of the surface at high excitation can be inferred from these data [21]. Since the present work tests our ideas about the relationship between the GDR and surface degrees of freedom in cold nuclei (i.e., at low temperature and angular momentum), it serves as a testing ground for their application in hot nuclei. We now address this issue by asking whether can one learn about the collective nature of the low-lying surface degrees of freedom through the study of the properties of the GDR. Said differently, does the GDR serve as a "fingerprint" for the nuclear surface? For the most part, the present data support this idea. Certainly, for the "extreme" nuclei in the transitional chain, namely, the spherical nucleus ^{142}Nd and deformed nucleus ^{150}Nd, both the photoabsorption and photon-scattering data directly reflect the shape and collective properties of the nuclear surface. The same can also be said of the soft vibrational nucleus ^{146}Nd. However, this is not true of ^{148}Nd, where both the photoabsorption and scattering data are equally well described whether the nucleus is treated as a weakly deformed rotator or as a soft spherical factor. In fact, it is quite likely that neither of these two extremes is the "correct" description of ^{148}Nd, which is expected to be a truly transitional nucleus. Nevertheless, both give an equally good accounting of the scattering data, indicating that in this case the properties of the GDR are a very poor indicator of the collective nature of the surface.

One final comment is in order. In the study of the GDR built on highly excited states, it is quite common to parametrize the GDR photoabsorption cross section as a sum of a few Lorentzian resonance lines. For data that can be fitted with a single Lorentzian, one concludes that the nucleus is spherical. If two Lorentzians are needed, then one concludes that the nucleus is deformed with axial symmetry, either prolate or oblate, depending on the relative strength in the lower component compared with the upper. And if three Lorentzians are needed, then one concludes that the nucleus is triaxial. Within the context of either the DCM or IBM, those simple conclusions do not follow. In fact, an inspection of Figs. 6 and 7 shows that the distribution of dipole strength is often much more complicated than implied by this simple picture, suggesting that one must be cautious in drawing strong conclusions about the shape of the nuclear surface based on a few-Lorentzian fit to the photoabsorption cross section.

V. SUMMARY

We have measured cross sections for the elastic and inelastic scattering of photons in the region of the GDR of the transitional chain of Nd isotopes ^{142,146,148,150}Nd.

The measurements utilized beams of quasimonochromatic tagged photons and good-resolution photon detectors in order to resolve the scattering into the ground and first few excited states. The cross sections were interpreted in the context of two nuclear structure models, the DCM and IBM, in which the photon-decay branches to excited states are a consequence of the coupling between the GDR and collective degrees of freedom associated with the nuclear surface. This represents the first test of the photon-decay predictions of these models across a complete transitional chain. We find that the predictions of both models are in excellent agreement with the measured scattering cross sections. Further, we find that the scattering into the ground and first excited states does not meaningfully discriminate between the two models. We suggest that this is not an experimental limitation, but rather a theoretical one due to the large phenomenological damping widths of the dipole states. On the other hand, scattering into higher levels could, in principle, discriminate, but the present data are not precise enough to select one model over the other. For the transitional nucleus ^{148}Nd, the data cannot easily select among several extreme models for the low-lying collective structure.

This research was supported by the National Science Foundation under Grant No. NSF PHY 89-21146.

*Present address: Department of Physics, Brookhaven National Laboratory, Upton, New York 11973.

[1] P. Carlos, H. Beil, R. Bergère, A. Leprêtre, and A. Veyssière, Nucl. Phys. **A172**, 437 (1971).
[2] J. Eisenberg and W. Greiner, *Nuclear Models* (North-Holland, Amsterdam, 1970), p. 331ff.
[3] T. J. Bowles, R. J. Holt, H. E. Jackson, R. M. Laszewski, R. D. McKeown, A. M. Nathan, and J. R. Specht, Phys. Rev. C **24**, 1940 (1981).
[4] A. M. Nathan, Phys. Rev. C **38**, 92 (1988).
[5] A. Arima and F. Iachello, in *Advances in Nuclear Physics,* edited by J. W. Negele and E. Vogt (Plenum, New York, 1984), Vol. 13, p. 141ff.
[6] I. Morrison and J. Weise, Nucl. Phys. **8**, 687 (1982).
[7] G. Maino, A. Ventura, L. Zuffi, and F. Iachello, Phys. Lett. **152**, 17 (1985).
[8] B. Harmatz and J. P. Shepard, Nucl. Data Sheets **20**, 396 (1977); T. W. Burrows, *ibid.* **14**, 444 (1975); L. K. Pekar, *ibid.* **42**, 111 (1984); E. der Mateosian, *ibid.* **48**, 345 (1986).
[9] C. M. Lederer and V. S. Shirley, *Table of Isotopes* (Wiley, New York, 1978).
[10] A. Bohr and B. Mottleson, *Nuclear Structure* (Benjamin, Reading, MA, 1975), Vol. II, p. 453ff.
[11] D. H. Wright, P. T. Debevec, L. J. Morford, and A. M. Nathan, Phys. Rev. C **32**, 1174 (1985).
[12] S. D. Hoblit, Ph.D. thesis, University of Illinois, 1988.
[13] W. R. Nelson, H. Hirayama, and D. W. Rogers, Report No. SLAC-265, 1985 (unpublished).
[14] V. Rezwani, G. Gneuss, and H. Arenhövel, Nucl. Phys. **A180**, 254 (1972).
[15] D. D. Warner and R. F. Casten, Phys. Rev. Lett. **48**, 1385 (1982).
[16] G. Maino, A. Ventura, L. Zuffi, and F. Iachello, Phys. Rev. C **30**, 2101 (1984).
[17] M. Danos and W. Greiner, Phys. Rev. **138**, B876 (1965).
[18] F. G. Scholtz and F. J. W. Hahne, Phys. Lett. **123B**, 147 (1983); Phys. Rev. C **34**, 693 (1986); Nucl. Phys. **A471**, 545 (1987).
[19] B. Fogelberg and G. Skarnemark, Nucl. Phys. **A453**, 15 (1986).
[20] A. Ahmed, G. Bomar, H. Crowell, J. H. Hamilton, H. Kawakami, C. F. Maguire, W. G. Nettles, R. B. Piercey, A. V. Ramayya, R. Soundranayagam, R. M. Ronningen, O. Scholten, and P. H. Stelson, Phys. Rev. C **37**, 1836 (1988).
[21] J. J. Gaardhoje, Nucl. Phys. **A488**, 261 (1988).